

Supplementary information

A silver-manganese dual cocatalyst for selective reduction of carbon dioxide into carbon monoxide over a potassium hexatitanate photocatalyst with water

Xing Zhu,^a Akira Yamamoto,^{a,b} Shota Imai,^c Atsuhiko Tanaka,^{d,e} Hiroshi Kominami,^d and Hisao Yoshida^{a,b,*}

^a Graduate School of Human and Environmental Studies, Kyoto University, Kyoto 606-8501, Japan

^b Elements Strategy Initiative for Catalysts and Batteries (ESICB), Kyoto University, Kyoto 615-8520, Japan

^c Molecular and Material Engineering, Interdisciplinary Graduate School of Science and Engineering, Kindai University, 3-4-1 Kowakae, Higashiosaka, Osaka 577-8502, Japan.

^d Department of Applied Chemistry, Faculty of Science and Engineering Kindai University, 3-4-1 Kowakae, Higashiosaka, Osaka 577-8502, Japan.

^e Precursory Research for Embryonic Science and Technology (PRESTO), Japan Science and Technology Agency (JST), 4-1-8 Honcho, Kawaguchi 332-0012, Japan

* Corresponding author: yoshida.hisao.2a@kyoto-u.ac.jp

06 Feb 2020 - note added after first publication: this Supplementary Information file replaces that originally published on 28 Sep 2019, in which the captions for Fig. S10 (e) and (f) were the wrong way around.

Contents

1. Experimental.....	2
1.1. Photocatalyst preparation	2
1.2. Characterization	2
1.3. Photocatalytic reaction.....	2
2. Results.....	3
2.1. XRD and SEM image of potassium hexatitanate	3
2.2. Photocatalytic reaction tests	4
2.3. Diffuse reflectance UV visible spectra	6
2.4. EXAFS spectra	6
2.5. SEM images and TEM-EDS mappings.....	7
References	

1. Experimental

1.1. Photocatalyst preparation

Potassium titanate ($K_2Ti_6O_{13}$, KTO) sample was prepared by a flux method.¹ The precursors, K_2CO_3 (Kishida) and TiO_2 (rutile, Kojundo), and a flux reagent KCl (Kishida) were mixed, where the molar ratio of K_2CO_3 to TiO_2 was 1:6, and that of KTO to KCl was 3:7. The mixture was put into a platinum crucible, heated in an electric muffle furnace with a rate of 200 K h^{-1} to 1273 K, held at this temperature for 10 h, and then cooled down at a rate of -100 K h^{-1} to 773 K, followed by being naturally cooled to room temperature in the furnace. The obtained powder was thoroughly washed with hot water (353 K, 500 mL) for 15 minutes and filtrated, and this washing step was repeated 4 times to remove the residual salt, then dried at 323 K for 24 hours.

Dual cocatalysts were loaded on the surface by a facile simultaneous photodeposition (PD) method.² Here, 1 g of the $K_2Ti_6O_{13}$ sample was dispersed in 400 mL of ion-exchanged water containing a required amount of precursors ($AgNO_3$, $Cr(NO_3)_2$, $Mn(NO_3)_2$, $Co(NO_3)_2$, and $Ni(NO_3)_2$, $PdCl_2$, $HAuCl_4$), and a bubbling flow of Ar gas was used to exclude the air for 1 hour before photoirradiation. Then the suspension was photoirradiated from a 100 W high-pressure Hg lamp with a bubbling flow of Ar gas for 3 h, followed by filtration and drying at room temperature.

1.2. Characterization

The loading amount of cocatalyst on the samples was evaluated by X-ray fluorescence analysis with an EDX-8000 (Shimadzu) using each experimentally obtained calibration curve, where the samples loaded by an impregnation method were used as references. The crystal structure of the samples was determined by powder X-ray diffraction with a Lab X XRD-6000 (Shimadzu). Morphologies of the samples were observed by scanning electron microscopy (SEM) with a JSM-890 (JEOL). Images of transmission electron microscopy (TEM) and scanning transmission electron microscopy (STEM) were taken by a JEOL JEM-2100F at 200 kV in the Joint Research Center of Kindai University. The sample was dispersed in methanol, dropped onto a carbon-coated copper grid, and dried at ambient temperature for 5 h. Diffuse reflectance UV-Vis spectrum was recorded by a V-670 (JASCO). Ag and Mn K-edge X-ray absorption fine structure (XAFS) were measured at NW-10C and BL-12C of the Photon Factory (KEK, Tsukuba, Japan), respectively. Most of the samples including the references were measured in a transmission mode, while the Mn K-edge XAFS spectra of the Mn(0.15)/KTO and Ag(1.0)-Mn(0.09)/KTO samples were measured in a fluorescence mode due to the extremely low amount of Mn species.

1.3. Photocatalytic reaction

The photocatalytic activity test of CO_2 reduction with water was carried out using a flow system with an inner-irradiation-type reaction vessel,³ as was shown in Fig. S1. Typical reaction conditions are as follows: The photocatalyst powder sample (0.3 g) was dispersed in ion-exchanged water (400 mL) containing 0.5 M

NaHCO_3 (pH=7), and suspended by magnetically stirring. Then, CO_2 was bubbled into the solution at a flow rate of 30 mL min^{-1} without irradiation for 1.5 hours. The photocatalytic reaction was conducted using a 100 W high-pressure mercury lamp. The light intensity was measured to be 22 mW cm^{-2} at a detecting wavelength of $254 \pm 10 \text{ nm}$. The reaction temperature was set at 290 K with cooling water. The amount of the products (H_2 , O_2 , and CO) in the outlet gas from the reactor were determined by using an on-line gas chromatograph (Shimadzu, GC-8A, TCD, a Shincarbon ST column, argon carrier).

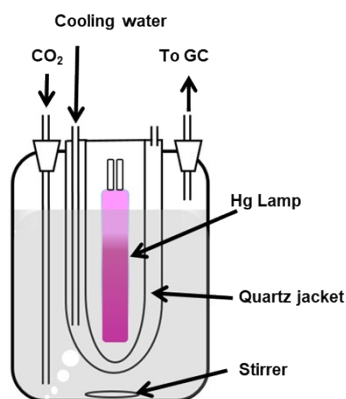


Fig. S1 The reactor set-up for the photocatalytic reaction test for CO_2 reduction with water under photoirradiation.

2. Results

2.1. XRD and SEM image of potassium hexatitanate

Fig. S2 shows XRD patterns of the obtained KTO sample and a $\text{K}_2\text{Ti}_6\text{O}_{13}$ reference from a database (ICSD#25712). The XRD pattern of the prepared KTO sample was consistent with that of the reference. It gives a correct diffraction pattern and no diffraction lines corresponding to other impurity phases, confirming that the prepared potassium hexatitanate was correctly fabricated by the flux method.

Fig. S3 shows that the KTO sample consisted of rod-like crystals with similar morphology and size.

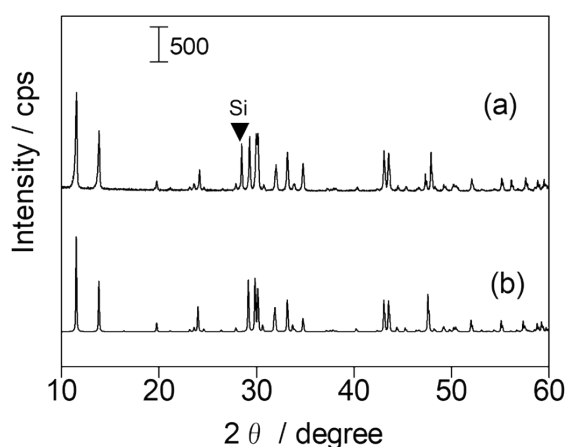


Fig. S2 XRD patterns of (a) the prepared KTO sample and (b) a reference data #25712 from ICSD database for $\text{K}_2\text{Ti}_6\text{O}_{13}$. A closed triangle indicates a diffraction from silicon powder mixed with the KTO sample to calibrate the angle.

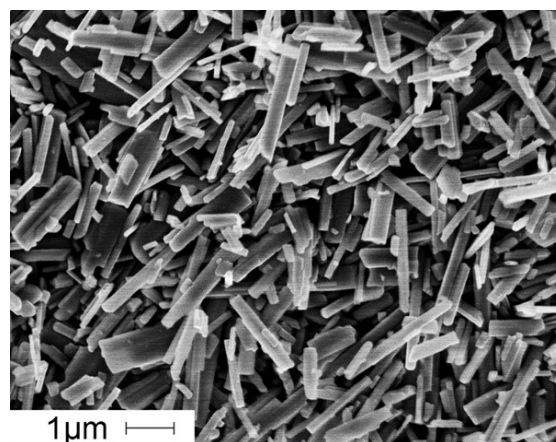


Fig. S3 SEM image of the prepared KTO sample.

2.2. Photocatalytic reaction tests

The results of photocatalytic reaction tests over eight samples loaded with different cocatalysts were shown in Fig. S4. The Ag(1.0)/KTO sample produced CO with high selectivity ($S_{CO}=94.8\%$). The samples with the Ag-Pd, Ag-Au, or Ag-Cu dual cocatalyst produced H_2 preferably, and other samples with the Ag-Cr, Ag-Ni, Ag-Co, or Ag-Mn dual cocatalyst formed predominantly CO with high selectivity more than 85%. As was well known, the precious metal cocatalysts, such as Pd and Pt cocatalyst,⁴ are very beneficial to the H_2 evolution, while the transition metal oxide cocatalysts such as MnO_x and CrO_x exhibit high activity for O_2 evolution.⁵ In the current study, the photocatalyst with a Ag- MnO_x dual cocatalyst exhibited the highest activity than other dual cocatalysts. In the present study the cocatalysts were loaded by a photodeposition method and the real loading amount of CrO_x , CoO_x and NiO_x were very limited. Thus, the deposition method and the amount of cocatalysts deposited are supposed to be the possible reasons for low activity. This remains further possibilities that other transition metal oxide species might exhibit high performance after each optimization.

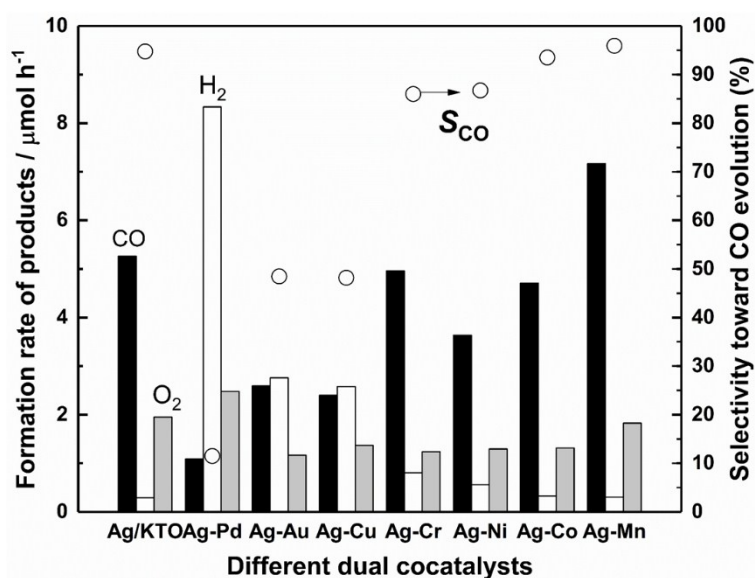


Fig. S4 Formation rates of CO (black bar), H_2 (white bar), and O_2 (grey bar) and the S_{CO} (open circles) in the photocatalytic CO_2 reduction with H_2O over the prepared KTO samples, (a) Ag(1.0)/KTO, (b) Ag(1.0)-Pd(1.0)/KTO, (c) Ag(1.0)-Au(0.85)/KTO, (d) Ag(1.0)-Cu(1.0)/KTO, (e) Ag(1.0)-Cr(0.006)/KTO, (f) Ag(1.0)-Ni(0.02)/KTO, (g) Ag(1.0)-Co(0.02)/KTO, and (h) Ag(1.0)-Mn(0.09)/KTO.

The photocatalytic reaction tests were conducted for the Ag-Mn/KTO samples with different Ag loading amount (Fig. S5). Although the same amount of Mn was added, the actually loaded amount of Mn was varied with the loading amount of Ag cocatalyst. It was found that the formation rate of CO first increased then decreased with the increasing loading amount of Ag cocatalyst. The samples with moderate loading amount in the range of 0.5–2.0 wt% of Ag and 0.10–0.13 wt% of Mn (Fig. S5, e–g) exhibited high photocatalytic activity for CO evolution. When the Ag loading amount is more than 2 wt%, the Ag particles would aggregate and the photocatalytic activity of CO_2 reduction would decrease.

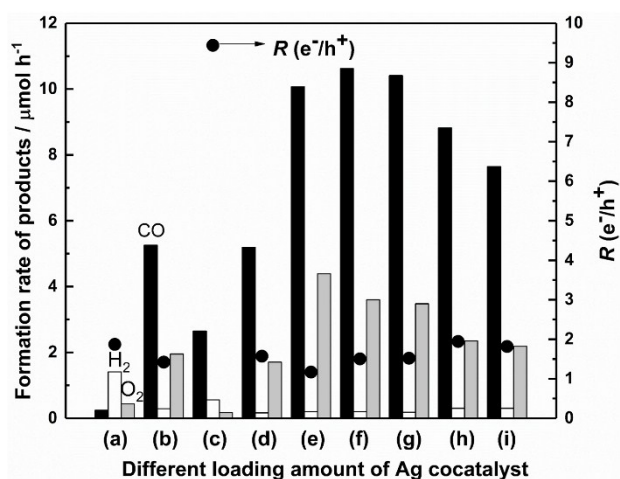


Fig. S5 Formation rate of CO, H₂, and O₂ and $R(e^-/h^+)$ in the photocatalytic CO₂ reduction over the Ag-Mn/KTO samples loaded with different amount of Ag cocatalyst, (a) bare KTO, (b) Ag(1.0)/KTO, (c) Ag(0.1)-Mn(0.21)/KTO, (d) Ag(0.3)-Mn(0.14)/KTO, (e) Ag(0.5)-Mn(0.13)/KTO, (f) Ag(1.0)-Mn(0.12)/KTO, (g) Ag(2.0)-Mn(0.10)/KTO, (h) Ag(3.0)-Mn(0.07)/KTO and (i) Ag(4.0)-Mn(0.06)/KTO.

The photocatalytic reaction tests were conducted for the Ag-Mn/KTO samples with different Mn loading amount (Fig. S6). It was found that the formation rate of CO first increased then decreased with the increasing loading amount of Mn cocatalyst, and the samples of the Mn loading amount in the range 0.12-0.14 wt% (Fig. S6, d and e) exhibited high formation rates of CO and O₂ with high selectivity such as 98%. Here, when the amount of MnO_x is low, the enhancement of O₂ evolution was not enough, although the activity was improved. When a large amount of Mn was loaded, the MnO_x species would aggregate and the photocatalytic activity would decrease.

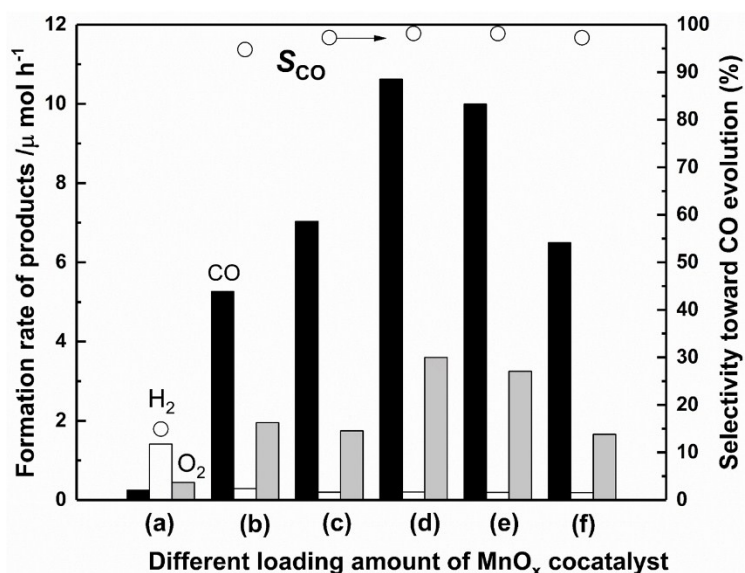


Fig. S6 Formation rate of CO, H₂, and O₂ and $S_{CO}(\%)$ in the photocatalytic CO₂ reduction over the Ag-Mn/KTO samples loaded with different Mn loading amount, (a) bare KTO, (b) Ag(1.0)/KTO, (c) Ag(1.0)-Mn(0.09)/KTO, (d) Ag(1.0)-Mn(0.12)/KTO, (e) Ag(1.0)-Mn(0.14)/KTO, and (f) Ag(1.0)-Mn(0.17)/KTO.

Some blank tests were carried out by using the Ag(0.5)-Mn(0.13)/KTO sample as shown in Table S1. No product was detected under dark conditions (Table S1, entry 2). Without a photocatalyst or without using a NaHCO₃ additive, only very low amounts of CO and H₂ were obtained (Table S1, entries 3 and 4), indicating that the photocatalyst and NaHCO₃ were both necessary to yield them sufficiently. And when a flow of argon gas was used instead of the flowing CO₂ gas (Table S1, entry 5), the CO evolution was also observed since CO₂ is formed from NaHCO₃ in the solution due to the equilibrium, but the rate was quite low, showing the predominant CO formation originates from molecular CO₂.

Table S1 Results of some blank tests for the photocatalytic CO₂ reduction with H₂O under different conditions.

Entry	conditions	Formation rate of products / $\mu\text{mol h}^{-1}$			$S_{\text{CO}}(\%)^b$
		CO	H ₂	O ₂	
1	standard conditions ^a	10.07	0.20	4.39	98.2
2	without irradiation	0.00	0.00	0.00	–
3	without photocatalyst	0.81	0.91	0.17	47.1
4	without NaHCO ₃	0.99	0.75	0.00	56.9
5	without CO ₂	1.63	0.19	0.75	89.6

^a Photocatalyst: the Ag(0.5)-Mn(0.13)/KTO sample, 0.3 g, reaction solution volume: 0.4 L, additive: 0.5 M NaHCO₃, CO₂ flow rate: 30 mL min⁻¹, light source: a 100 W high pressure Hg lamp. ^b Selectivity to CO, $S_{\text{CO}}(\%) = 100 \times R_{\text{CO}} / (R_{\text{CO}} + R_{\text{H}_2})$, where R_{CO} and R_{H_2} are the production rate of CO and H₂, respectively.

The recycle tests were performed to confirm the stability and durability of the prepared sample repeatedly for two time under the same conditions. The first run is shown in Fig. 1 and the second one (reused test) is presented below as Fig. S7. Also in the second run, almost the same formation rates of CO and H₂ were achieved, while there was a slight loss by a ca.10% O₂ evolution activity. This may due to the ca.15% loss of both Ag and MnO_x cocatalyst, which was confirmed by the XRF.

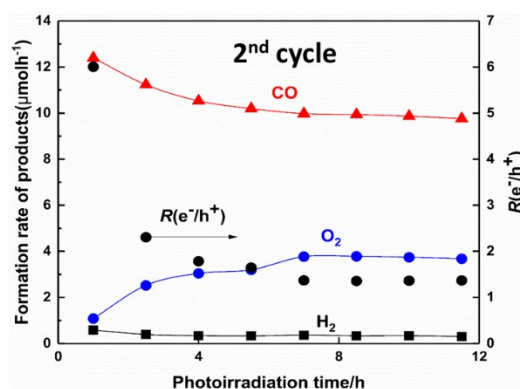


Fig. S7 Time course of the production rates of CO, H₂, and O₂, and R(e⁻/h⁺) with the Ag(0.5)-Mn(0.13)/KTO sample in the photocatalytic CO₂ reduction test as the second run after the first run shown in Fig. 1.

2.3. Diffuse reflectance UV visible spectra

DR UV-visible spectra of the four samples are shown in Fig. S7. In the spectrum of the Mn(0.15)/KTO sample (Fig. S7b), a broad and very weak absorption band was observed, which is consistent with the fact that transition metal oxide such as manganese oxide usually shows grey color. Although the assignment of the small band observed at around 390 nm for the Ag(1.0)/KTO sample was not clarified yet (Fig. S7c), it may originate from the interaction of Ag species with the surface of KTO in the absence of the surface modification with Mn species. Other explanations are mentioned in the main text.

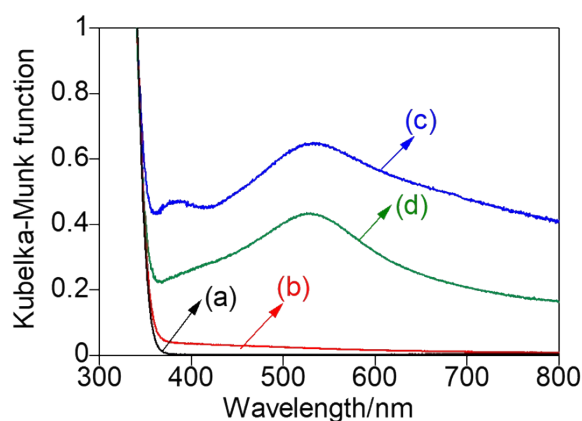


Fig. S8 DR UV-vis spectra of the prepared samples, (a) bare KTO, (b) Mn(0.15)/KTO, (c) Ag(1.0)/KTO, and (d) Ag(1.0)-Mn(0.09)/KTO.

2.4. EXAFS spectra

Explanations for Fig. S9 and S10 are described in the main text.

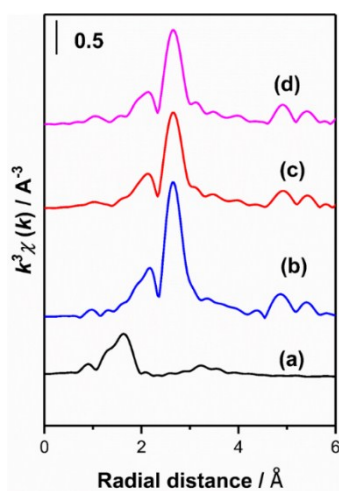


Fig. S9 Fourier-transforms of Ag K-edge EXAFS spectra of (a) Ag₂O, (b) Ag foil, (c) the Ag(1.0)/KTO sample, and (d) the Ag(1.0)-Mn(0.09)/KTO sample.

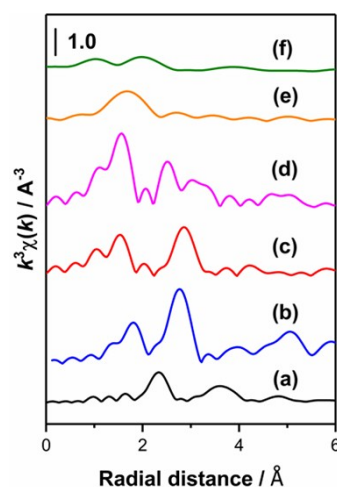


Fig. S10 Fourier-transforms of Mn K-edge EXAFS spectra of (a) Mn foil, (b) MnO, (c) Mn₂O₃, (d) MnO₂, (e) the Ag(1.0)-Mn(0.09)/KTO sample, and (f) the Mn(0.15)/KTO sample.

2.5. SEM images and TEM-EDS mappings

The SEM images of the prepared Ag(1.0)/KTO and Ag(1.0)-Mn(0.09)/KTO samples were shown in Fig. S11. The Ag nanoparticles loaded on the Ag(1.0)/KTO sample were clearly observed. Nanoparticles were also observed for the Ag(1.0)-Mn(0.09)/KTO samples, although it is very hard to distinguish the Ag cocatalyst and MnO_x cocatalyst.

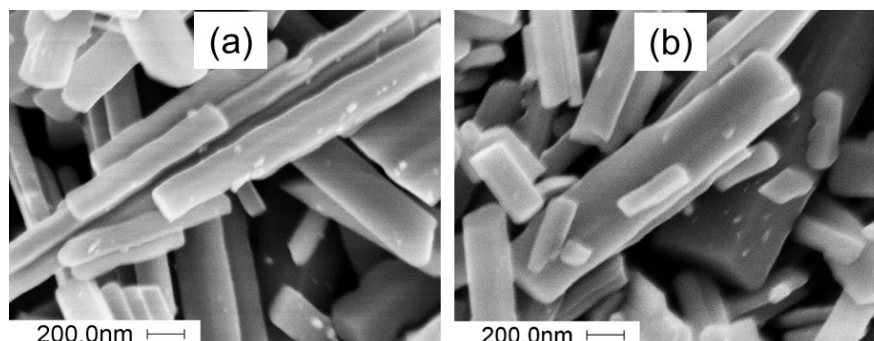


Fig. S11 SEM images of (a) the Ag(1.0)/KTO sample, and (b) the Ag(1.0)-Mn(0.09)/KTO sample.

Fig. S12a and S12b show the TEM images of the prepared Ag(1.0)/KTO and Ag(1.0)-Mn(0.09)/KTO samples, respectively, where nanoparticles were observed on the surface of these two samples. As confirmed by EDS mapping shown at the right side of TEM images, the observed nanoparticles were assignable to Ag nanoparticles. Although some dots were found in each EDS mapping of Mn, they were assignable to not Mn species but the background noise because these dots are observed even in the area without any material, i.e., upper side in Fig. S12(a) and upper middle area in Fig. S12(b). Therefore, the Mn species were not confirmed by the EDS mapping for both the Ag(1.0)/KTO and Ag(1.0)-Mn(0.09)/KTO samples, which may be due to the extremely low concentration as well as the amorphous and well dispersed structure.

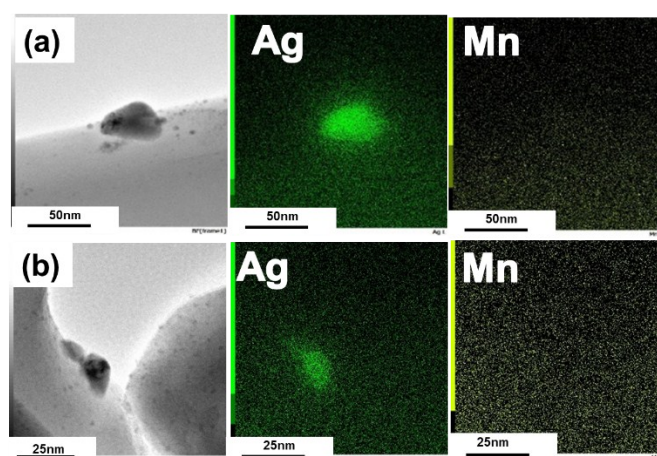


Fig. S12 TEM images and EDS mappings of (a) the Ag(1.0)/KTO sample, and (b) the Ag(1.0)-Mn(0.09)/KTO sample.

Table S2 shows the comparison of CO formation rate and selectivity for photocatalytic CO₂ reduction with H₂O in reported researches, although the reaction conditions were quite different from each other, for example using a large scale reactor, a high-powered lamp, and a large amount of water and photocatalyst. Among them, the current photocatalytic system shows a moderate activity and the highest selectivity.

Table S2 Reported photocatalytic performances in photocatalytic CO₂ reduction with H₂O.

Entry	Photocatalyst	Weight of sample (g)	Volume of water (L)	High pressure mercury Lamp (W)	CO evolution activity (μmol h ⁻¹)	CO selectivity (%)
1 ^{6a}	Ag/BaLa ₄ Ti ₄ O ₁₅	0.3	0.36	400	22	67
2 ^{6b}	Ba ₂ Li _{2/3} Ti _{16/3} O ₁₃	1.0	1.8	400	1.6	12
3 ^{6c}	Ag/SrNb ₂ O ₆	0.5	1.0	400	36	96
4 ^{6d}	Ag/ZnGa ₂ O ₄ /Ga ₂ O ₃	1.0	1.0	400	108	92
5 ^{1a}	Ag/Na ₂ Ti ₆ O ₁₃	0.3	0.35	100	2.8	82
6 (Current study)	Ag-Mn/K ₂ Ti ₆ O ₁₃	0.3	0.4	100	10	98

References

- 1 (a) X. Zhu, A. Anzai, A. Yamamoto and H. Yoshida, *Appl. Catal. B Environ.*, 2019, **243**, 47. (b) H. Yoshida, M. Sato, N. Fukuo, L. Zhang, T. Yoshida, Y. Yamamoto, T. Morikawa, T. Kajino, M. Sakano, T. Sekito, S. Matsumoto, H. Hirata, *Catal. Today*, 2017, **303**, 296.
- 2 R. Pang, K. Teramura, H. Tatsumi, H. Asakura, S. Hosokawa and T. Tanaka, *Chem. Commun.*, 2018, **54**, 1053.
- 3 A. Anzai, N. Fukuo, A. Yamamoto and H. Yoshida, *Catal. Commun.*, 2017, **100**, 134.
- 4 (a) Y. Ma, R. Chong, F. Zhang, Q. Xu, S. Shen, H. Han and C. Li. *Phys.Chem.Chem.Phys.*, 2014, **16**, 17734. (b) R. Pang, K. Teramura, H. Tatsumi, H. Asakura, S. Hosokawa and T. Tanaka, *Chem. Commun.*, 2018, **54**, 1053.
- 5 (a) J. Yang, D. Wang, H. Han and C. Li, *Acc. Chem. Res.*, 2013, **46**, 1900. (b) R. Li, F. Zhang, D. Wang, J. Yang, M. Li, J. Zhu, X. Zhou, H. Han and C. Li, *Nat. Commun.*, 2013, **4**, 1432.
- 6 (a) K. Iizuka, T. Wato, Y. Miseki, K. Saito and A. Kudo, *J. Am. Chem. Soc.*, 2011, **133**, 20863. (b) L. F. Garay-Rodríguez, H. Yoshida, and L. M. Torres-Martínez, *Dalton Trans.*, 2019, **48**, 12105. (c) R. Pang, K. Teramura, H. Asakura, S. Hosokawa and T. Tanaka, *Appl. Catal. B Environ.*, 2017, **218**, 770. (d) Z. Wang, K. Teramura, Z. Huang, S. Hosokawa, Y. Sakata and T. Tanaka, *Catal. Sci. Technol.*, 2016, **6**, 1025.